HHS Public Access

Author manuscript

Dent Mater. Author manuscript; available in PMC 2020 October 02.

Published in final edited form as:

Dent Mater. 2020 October ; 36(10): 1303–1313. doi:10.1016/j.dental.2020.06.003.

Bioactivating a bone substitute accelerates graft incorporation in a murine model of vertical ridge augmentation

Jinlong Chen[a,b], **Xue Yuan**[b], **Zhijun Li**[b,c], **Daniel J. Bahat**[b,d], **Jill A. Helms**[b,*]

[a]State Key Laboratory of Oral Diseases & National Clinical Research Center for Oral Diseases, West China Hospital of Stomatology, Sichuan University, Chengdu, China

[b]Division of Plastic and Reconstructive Surgery, Department of Surgery, Stanford University School of Medicine, Palo Alto, CA, USA

[c]Department of Orthopedics, Tianjin Medical University General Hospital, Tianjin, China

[d]Sidney Kimmel Medical College, Thomas Jefferson University, Philadelphia, PA, USA

Abstract

Objective.—Compared to autologous bone grafts, allogeneic bone grafts integrate slowly, which can adversely affect clinical outcomes. Here, our goal was to understand the molecular mechanisms underlying graft incorporation, and then test clinically feasible methods to accelerate this process.

Methods.—Wild-type and transgenic Wnt "reporter" mice were used in a vertical ridge augmentation procedure. The surgery consisted of tunneling procedure to elevate the maxillary edentulous ridge periosteum, followed by the insertion of bone graft. Micro-computed tomographic imaging, and molecular/cellular analyses were used to follow the bone graft over time. Sclerostin null mice, and mice carrying an activated form of β-catenin were evaluated to understand how elevated Wnt signaling impacted edentulous ridge height and based on these data, a biomimetic strategy was employed to combine bone graft particles with a formulation of recombinant WNT protein. Thereafter, the rate of graft incorporation was evaluated.

Results.—Tunneling activated osteoprogenitor cell proliferation from the periosteum. If graft particles were present, then osteoprogenitor cells attached to the matrix and gave rise to new bone that augmented edentulous ridge height. Graft particles alone did not stimulate osteoprogenitor cell proliferation. Based on the thicker edentulous ridges in mice with amplified Wnt signaling, a strategy was undertaken to load bone graft particles with WNT; this combination was sufficient to accelerate the initial step of graft incorporation.

Significance.—Local delivery of a WNT protein therapeutic has the potential to accelerate graft incorporation, and thus shorten the time to when the graft can support a dental implant.

*Corresponding author at: Stanford University, 1651 Page Mill Road, Palo Alto, CA 94304, USA., jhelms@stanford.edu (J.A. Helms).

Appendix A. Supplementary data

Supplementary material related to this article can be found, in the online version, at doi:https://doi.org/10.1016/j.dental.2020.06.003.

Keywords

Bone substitutes; Alveolar bone grafting; Edentulous jaw; Bone regeneration; Wnt3A protein

1. Introduction

For decades, autologous bone has served as the standard of care for the reconstruction of large bony defects [1]. Autologous bone grafts (autografts) contain osteoprogenitor cells, a mineralized matrix scaffold, and growth factors that collectively allow the graft to seamlessly integrate at the site of transplantation [2]. Nonetheless, there are disadvantages to autografting: first, there is persistent discomfort that accompanies the harvesting of bone from the iliac crest [3,4]. Second, there is often a limited amount of autograft that can be harvested [5]. Third, there is the issue of osteogenic potential: the older the patient, the less osteogenic the autograft becomes [6]. Finally, there is the issue of resorption: despite initial gains, over time, autografted sites undergo a significant loss in volume [7,8].

Collectively, these disadvantages have made way for the development of bone graft extenders (reviewed in [9]). Their ease of use and unlimited quantities are two major advantages, but all allogeneic bone graft extenders must undergo deproteinization and decellularization to ensure immune-compatibility [10], Since they are devoid of stem/osteoprogenitor cells, and pro-osteogenic proteins, new bone tends to form very slowly around allografts [11,12]. This delayed graft incorporation is problematic and contributes to greater variability in clinical outcomes when allografts are used [13]. We reasoned that if the rate of new bone formation could be accelerated around allografts, then these materials may effectively replace the need for autografts.

WNT proteins are potent, pro-osteogenic factors [14–16] that stimulate osteogenesis by activating the osteogenic transcription factor Runx2 [17–19], and repressing bone-resorbing pathways via a RANKL-dependent mechanism [20,21]. WNT proteins, however, are lipophilic and thus aggregate in aqueous *in vivo* environments. To prevent loss of activity, our laboratory developed a liposomal formulation of WNT3A e.g., L-WNT3A [22–24]. The liposome interacts with the glycosylated, palmitoylated modifications on WNT proteins, which are essential for Wnt signaling activity [25]. Liposomal packaging stabilizes the WNT protein, extending its half-life *in vivo* from minutes to multiple hours [22]. *in vivo*, L-WNT3A activates osteoprogenitor cells, leading to their accelerated differentiation into matrix-secreting osteoblasts; consequently, we reasoned that combining this protein therapeutic with a non-resorbing allogeneic bone matrix scaffold might promote the activation of endogenous Wnt-responsive osteoprogenitor cells at the site of grafting, which in turn would accelerate the rate of new bone formation around the allograft.

We tested this possibility in a craniomaxillofacial procedure where allograft materials are used to increase the vertical dimension of an atrophied maxilla or mandible to support the placement of an implant [26]. A vertical ridge augmentation procedure was performed in the murine edentulous ridge, which lies between the first molar and incisors and is comprised of dense lamellar bone, similar to an atrophied human maxillae or mandible [26]. This region was large enough to permit the insertion of micro-forceps to create a periosteal tunnel, into

which bone graft particles could be inserted. The fate(s) of Wnt-responsive cells around the particles, and the effects of L-WNT3A, could then be monitored over time.

2. Materials and methods

2.1. Animals

Experimental protocols followed ARRIVE guidelines and were approved by the Stanford Committee on Animal Research (#13146). Wild-type and *Axin2*$^{CreERT2/+}$;*R26*$^{mTmG/+}$ mice (#018867 and #007576) were purchased from Jackson Laboratories. Both genders were used. All mice were between 6–8 weeks old at the initiation of the experiment.

A strain of Wnt reporter mice (*Axin2*$^{CreERT2/+}$;*R26*$^{mTmG/+}$) was employed in some experiments. In this strain, Cre expression is under the control of the Wnt target gene, *Axin2* [27]. Cre mediated recombination was induced by intraperitoneal delivery of tamoxifen (4 mg/25 g body weight); thereafter, Wnt-responsive cells are identifiable by expression of green fluorescent protein (GFP). Descendants arising from the initial population of Wnt-responsive cells are also labelled with GFP, which allowed for the unambiguous identification of Wnt-responsive cells in the periosteum. In our experiments, tamoxifen was delivered intraperitoneally for 3 consecutive days; animals were sacrificed 7 days after the last injection.

DaβcatOt mice and Sost$^{-/-}$ mice were generated in the laboratory of Dr. Teresita Bellido, whose protocol was approved by the Institutional Animal Care and Use Committee of Indiana University School of Medicine. DaβcatOt mice were generated as described [28], by crossing *dentin matrix acidic phosphoprotein 1* (*DMP1*)−8kb-Cre mice with *Catnb*$^{lox(ex3)}$ mice in which LoxP sites flank exon 3 that encodes for β-catenin degradation. *DMP1−8kb-Cre*$^{+/-}$ mice were crossed with *Catnb*$^{lox(ex3)/lox(ex3)}$ mice to generate *Catnb*$^{lox(ex3)/+}$; *DMP1−8kb-Cre*$^{+/-}$ (DaβcatOt mutant mice) and *Catnb*$^{lox(ex3)/+}$ mice (DaβcatOt control) mice.Sost$^{-/-}$ mice carried a targeted disruption of the SOST coding region and were generated as described [28].

2.2. L-WNT3A formulation and Wnt reporter activity assay

L-WNT3A was prepared as described in detail [22]. In brief, recombinant human WNT3A protein was combined with pre-formed DMPC:cholesterol (90:10) liposomes and incubated at room temperature for 2 h to generate WNT-lipid nanoparticles [22]. An identical liposomal formulation of phosphate buffered saline e.g., L-PBS was manufactured and used as a control.

The activity of L-WNT3A used here was validated using a cell-based potency LSL assay, in which mouse LSL cells were stably transfected with a Wnt-responsive luciferase reporter plasmid, pSuperTOPFlash (Addgene) containing 3 TCF/LEF binding sites regulating expression of luciferase. When LSL cells are exposed to L-WNT3A, the Wnt protein binds to Frizzled (Fz) receptors on the surface of the LSL cells, which initiates a cascade of Wnt-dependent intracellular events [29] that leads to the expression of luciferase [30]. After exposure to the Wnt stimulus, LSL cells were incubated for an additional 18 h at 37 °C, 5% CO_2 in 1 × DMEM (Invitrogen), 10 % FBS (Gibco), and 1% Penicillin/Streptomycin (P/S,

Mediatech). Then prior to quantification, cells were washed to remove exogenous Wnt and lysed with Lysis Buffer (Applied Biosystems). Luciferin was added to the culture medium, and underwent cleavage by luciferase; the energy released by this reaction was in the form of light [31] that was detected by a dual light reader. L-WNT3A potency was defined by comparing the readouts of samples to that of a reference standard consisting of recombinant human WNT3A protein (StemR&D), tested at known concentrations.

2.3. Allograft preparation and treatment with L-WNT3A

To allow placement in a mouse surgical site, bone matrix was placed into a mortar and ground with a pestle into smaller particles e.g., ~15–200 μm. Graft particles were then soaked in either L-WNT3A (concentration =0.3 ng/μL) or L-PBS at 4 °C for 15 min. To measure entrapment and release of active L-WNT3A, particles were removed from their solutions and placed onto LSL cells which were seeded at 50,000 cells/well in a 4-well chamber slide (Thermo) and allowed to recover for 4 h. After 18 h, cells were fixed in 4% PFA then immunostained for luciferase expression (see immunostaining described below). Cell nuclei were counter-stained with DAPI. Negative and positive control wells were treated with L-PBS and L-WNT3A, respectively, at a concentration of 10 μL in 100 μL total culture medium volume.

Quantification of Wnt activity in response to L-WNT3A delivered via bone graft particles was performed using Adobe Photoshop and ImageJ. Three samples co-cultured with L-WNT3A soaked bone graft were included. The first ROI was defined as an annulus around the bone graft particle with a width of 150 μm, while the second was defined as the annulus around the first annulus with the same width. Total cell numbers were counted using particle analysis in ImageJ, while the numbers of luciferase^{+ve} cells were counted manually. Then the percentage of luciferase^{+ve} cells was calculated.

2.4. Subperiosteal tunneling and bone graft placement

A vertical ridge augmentation procedure was performed using bone graft particles. Prior to the tunneling and/or grafting procedure, mice were anesthetized, and the mouth was rinsed using povidone-iodine solution for 1 min. A full-thickness incision was made between the first and second rugae, perpendicular to the maxillary bone surface. Micro-forceps were used to reflect the periosteum towards the maxillary first molar. Bone graft particles, either treated with L-WNT3A or with L-PBS (as above), were gently inserted into the tunnel. The surgical site was closed with non-absorbable single interrupted sutures (Ethilon nylon suture black monofilament 8–0, Johnson & Johnson Medical). Mice were fed provided regular hard-food chow (#2918, Envigo) and water ad libitum. Mice were sacrificed at timepoints indicated (see Appendix Table 1 for experimental groups, timepoints, and sample sizes).

2.5. Micro-computed tomography (μCT)

Samples were collected after euthanasia. The maxillae were split sagittally with a sharp blade. Tissues were fixed in 4% paraformaldehyde overnight at 4 °C. Three-dimensional μCT scanning and analyses followed published guidelines [32]. Scanning was performed using a μCT data-acquisition system (VivaCT 40, Scanco) at 10.5 μm voxel size (70 kV, 115 μA, 300 ms integration time). Three-dimensional reconstruction and volume rendering were

carried out using Avizo (FEI, Hillsboro, OR), Dataviewer (SkyScan) software and ImageJ (NIH, Bethesda, MD) software. Bone morphometry was evaluated using CTAn software (SkyScan, Belgium). Images were organized using Adobe Photoshop and Adobe Illustrator.

2.6. Tissue collection, processing and histology

Following the μCT imaging, samples were transferred to a microwave oven (Ted Pella, Redding, CA), in which a circulating 10 % ethylenediamine tetraacetic acid solution was held for decalcification. After a 2-week demineralization period, specimens were dehydrated through an ascending ethanol series then paraffin-embedded. 8μm-thick sagittal sections were cut and collected on Superfrost-plus slides for histology including Aniline blue, Masson's Trichrome, Movat's pentachrome, and Picro-sirius red staining, which followed published protocols [27].

2.7. Immunostaining

Immunostaining followed published protocols [33]. In brief, tissue sections were de-paraffinized then permeabilized with 0.5 % TritonX-100. Antigen retrieval was performed using Antigen Unmasking Solution (Vector Labs), following which slides were blocked with 5% goat serum (Vector S-1000) for 1 h at room temperature then incubated with primary antibodies overnight at 4 °C. After washing with PBS, slides were incubated with Cyanine5 conjugated goat anti-rabbit secondary antibody (Invitrogen, A-10523) for 30 min, then mounted with 4′,6-diamidino-2-phenylindole (DAPI) mounting medium (Vector Labs). Primary antibodies used in this study include anti-luciferase antibody (1:1000, ab21176, Abcam), anti-PCNA (1:5000; ab18197, Abcam), anti-Runx2 (1:1000; ab192256, Abcam), and anti-green fluorescent protein (GFP) (1:400; 2956S, Cell Signaling Technology).

2.8. Alkaline phosphatase (ALP) and Tartrate-resistant acid phosphatase (TRAP) activity

To detect ALP activity, tissue sections were treated with ALP-detection solution containing BCIP (5-bromo-4-chloro-3-indolyl phosphate; Roche, #11383221001) and NBT (nitro blue tetrazolium chloride; Roche, #11383213001) according to the manufacturer's instructions. TRAP activity was observed using a leukocyte acid phosphatase staining kit (catalog #386A-1 KT, Sigma-Aldrich). Tissue sections were processed according to the manufacturer's instructions.

2.9. Histomorphometric analyses

Histomorphometric measurements were performed using Adobe Photoshop. A minimum of 3 grafted sites/time point were analyzed for each treatment group. For each site, a minimum of three aniline blue-stained sagittal tissue sections, which included the mesial labial root as a landmark, were used to quantify maxillary bone thickness, and augmented thickness. Each tissue section was photographed using a Leica digital image system at 20x magnification. To obtain the augmented height, the region of newly formed bone was selected manually in Photoshop, then the area and width of the selected pixels was recorded using the measurement log. The average augmented thickness was calculated by dividing the area selected by its width. In addition, the area occupied by the bone graft particles was also

manually selected and recorded. From these measurements, the composition e.g., particles versus new bone of the total augmented region was determined.

To evaluate Runx2 expression in response to L-PBS versus L-WNT3A treatment, 3 graft sites from each treatment group were analyzed. From each site, at least 3 sagittal tissue sections were analyzed. The lasso tool in Adobe Photoshop was used to select a region of interest (ROI), which was the "pocket" area generated by the tunneling procedure. Within this ROI, the space occupied by bone graft particles was excluded. The number of $Runx2^{+ve}$ cells and the total number of the other cells (identified by DAPI) were then counted, and the ratio of $Runx2^{+ve}$ to total cells was then calculated.

To visualize collagen organization, 3 graft sites were selected from the L-PBS group and 3 graft sites from the L-WNT3A group, then 3 sagittal tissue sections from each of the specimens were analyzed. Picro-sirius red stained slides were viewed under polarized light using a Leica digital image system at 20x magnification. The same "pocket" ROI was selected, as described above. With the color analysis tool in Photoshop, the number of orange/red pixels, corresponding to mature collagen fibers, were selected using a uniform color range and counted, and the same was done for green pixels, which corresponded to immature collagen fibers. Then, the total pixels within the same ROI was determined. Mature/immature collagen fibers were expressed as a percentage of their respective pixels/ total pixels in the ROI.

2.10. Statistical analysis

Results were presented as mean ± standard deviation. All statistical analyses were performed using the Prism 7.0 (GraphPad Software). Comparisons of immunopositive cell percentage and collagen organization were analyzed using the two-tailed Student's T-test. Comparisons of augmented maxillary height with non-treated bone grafts were based on a one-way ANOVA followed by Turkey's post-hoc testing. While, comparisons of augmented maxillary height with L-WNT3A/L-PBS treated bone graft were performed based on a two-way ANOVA with Geisser-Greenhouse correction, followed by Turkey's post-hoc testing for multiple comparisons. Significance was attained at $p < 0.05$ (*), $p < 0.01$(**), and $p < 0.001$(***). An online tool, designed for calculating the minimum sample size for adequate study power, was employed: https://clincalc.com/stats/SampleSize.aspx.

3. Results

3.1. Establishing a rodent model of vertical ridge augmentation via tunneling and bone grafting procedures

On atrophic maxillae and mandibles, vertical ridge augmentation is performed when there is insufficient bone volume to support an implant. To mimic this clinical scenario, the rodent edentulous ridge was selected. Its thin, lamellar, dense bone (Fig. 1A) resembles the type of bone clinicians usually encounter when performing vertical ridge augmentation [26]. Bone grafting was accomplished using bovine mineralized matrix particles (see Methods). In most cases (14/16) the bone graft remained on the crest of the edentulous ridge (arrows, Fig. 1B), stabilized there by a soft tissue envelope produced via a subperiosteal tunneling procedure.

In cases where the graft shifted from its original position (N = 2), samples were excluded from further analyses.

We inspected the clinical response to vertical ridge augmentation, separating the tunneling component of the surgery from the grafting procedure. Intact tissues served as controls (Supplemental Fig. 2A). The tunneling procedure resulted in an irregular border of the maxillary bone (dotted white line, Fig. 1C compared with controls, Supplemental Fig. 2A). In cases where bone graft had been inserted into the soft tissue envelope, graft particles (dotted black lines, Fig. 1D) were observed next to the irregular maxillary bone and in some instances, new woven bone was detected near the particles (green arrowheads, Fig. 1E). Over time, bone graft particles near to the maxillary bone became embedded in new bone matrix (green arrowheads, Fig. 1F,G).

Using picrosirius red staining and polarized light, new bone matrix was easily distinguished from pre-existing maxillary bone by virtue of its immature collagen organization (Fig. 1H). Quantitative μCT imaging on post-surgery day (PSD) 28 illustrated the extent to which the bone graft was fully incorporated into new bone (arrows, Fig. 1I). Vertical maxillary bone height was quantified as a function of time post-grafting: between PSD0 and 9, there was minimal change in the thickness of the maxillary edentulous ridge (Fig. 1J). By PSD14, the grafted ridge was ~20 % thicker and by PSD28, the ridge height had more than doubled, i.e. increased by 141 % of its original thickness (Fig. 1J). Some of this vertical gain in height was directly due to the volume of the graft particles, and some was due to new bone formation; we analyzed the ratio and found that of the augmented bone volume, nearly 60 % was due exclusively to new bone formation (Fig. 1K). The remaining 41 % of augmented bone volume was due to the particles themselves.

Our next analyses focused on pinpointing the source of this new bone. One early clue came from an examination of the intact maxillary periosteum (Fig. 1L). Compared to the nasal surface (denoted n po), the periosteum on the oral surface (o po) was noticeably thicker and densely cellular (Fig. 1L,M). Periostea are niches for osteoprogenitor cells [34,35], which suggested that the new bone that gradually enveloped the graft particles might arise from this source. We therefore focused on how oral periosteum responded to tunneling and grafting procedures.

3.2. Tunneling activates osteoprogenitor proliferation in the periosteum

The periosteum was noticeably thicker following the tunneling procedure (compare Fig. 2A with B and C). The thicker periosteum was a site of active mineralization (compare Fig. 2D with E and F). This expansion in ALP activity caused by tunneling correlated with increased mitotic activity, as shown by PCNA immunostaining (compare Fig. 2G with H and I). These proliferating cells were osteoprogenitors, as shown by the distribution of $Runx2^{+ve}$ cells (compare Fig. 2J with K and L).

The presence of the bone graft particles had a dramatic effect on the distribution of proliferating osteoprogenitor cells: rather than remaining close to the native bone surface, if bone graft was used, $PCNA^{+ve}$, $Runx2^{+ve}$ cells encircled the particles (compare Fig. 2H with I and K with L). Clearly then, the presence of a mineralized matrix was sufficient to cause

the migration of osteoprogenitor cells away from their site of origin. We also found that $PCNA^{+ve}$, $Runx2^{+ve}$ osteoprogenitor cells were only increased in number if the periosteum was elevated off the bone surface: creating a connective tissue tunnel that left the periosteum attached to the bone did not lead to osteoprogenitor cell proliferation (not shown). Even creating a connective tissue tunnel and introducing graft particles was not sufficient to activate osteoprogenitor cell proliferation (Supplemental Fig. 3). Collectively, these data demonstrated that elevating the periosteum led to the proliferation of osteoprogenitor cells and if a graft were present then these new osteoprogenitor cells enveloped and attached the particles.

3.3. Enhanced Wnt signaling correlates with bone accrual

What signals were responsible for triggering the proliferation of osteoprogenitor cells in the injured periosteum? In the intact state, the periosteum is Wnt-responsive (Fig. 3A,B) and at least some of these Wnt-responsive cells co-stain for Runx2 (Fig. 3C). We reasoned that if Wnt signaling was critical for the proliferation of osteoprogenitor cells and bone accrual, then genetic models of elevated Wnt signaling should manifest as having thicker periostea and thicker edentulous ridges. We first evaluated mice carrying null mutations in the Wnt inhibitor, Sclerostin, which have elevated endogenous Wnt signaling [36]. Compared to wild-type mice (Fig. 3D–F), $Sost^{-/-}$ mice had a significantly thicker edentulous ridge (Fig. 3G–I; quantified in M) but not a noticeably thicker periosteum. We therefore evaluated a second genetic model of amplified Wnt signaling, e.g., $da\beta cat^{Ot}$ mice, which carry an activated form of β-catenin [37]. $Da\beta cat^{Ot}$ mice not only had a significantly thicker edentulous ridge (Fig. 3J,K; quantified in M), but also a noticeably thicker periosteum (Fig. 3L).

3.4. Use of a WNT-bioactivated graft accelerated bone accrual

Deletion of SOST and over-expression of activated β-catenin were genetic strategies to increase Wnt signaling; we under took a clinically feasible method of increasing Wnt signaling around bone graft particles. WNT liposomes are ~80 nm in diameter, and the average pore size in the bone graft was ~1 μm; therefore, we incubated the particles in L-WNT3A, theorizing that at least some of the protein therapeutic might become entrapped in the pores and then leach out over time. To test entrapment and release, we used an LSL cell assay. LSL cells are engineered to express luciferase in response to a Wnt stimulus [22]. The specificity of the luciferase response, and the activity of L-WNT3A, were both demonstrated (Fig. 4A,B).

Bone graft particles were then soaked in L-PBS or L-WNT3A; after 15 min, the treated particles were transferred onto LSL cells. LSL cells incubated with L-PBS treated bone graft particles did not express luciferase (Fig. 4C). In contrast, L-WNT3A treated bone particles were surrounded by a halo of luciferase-expressing cells (Fig. 4D). The luciferase-expressing cells were contained within a 150 μm zone surrounding the particles (Fig. 4E). These data demonstrated that bone graft particles could entrap and then release active L-WNT3A.

We tested the effects of L-WNT3A-bioactivated bone graft particles *in vivo*. L-PBS and L-WNT3A treated bone graft particles were prepared and placed onto the edentulous ridge. Six days later, significantly more $Runx2^{+ve}$ osteoprogenitor cells were detected around WNT-bioactivated particles (compare Fig. 4F,G; quantified in H). Collagen matrix appeared to more mature around the WNT-bioactivated particles, as shown by Picrosirius red staining (Fig. 4I,J; quantified in K).

By PSD9, more bone surrounded the WNT-bioactivated particles (Fig. 4L,M; quantified in P) but by PSD14 the amount of new bone appeared to be equivalent between the experimental groups (Fig. 4N,O; quantified in P). Collectively, these data demonstrated a significant but transient acceleration in new bone formation around WNT-bioactivated bone graft particles.

4. Discussion

4.1. A rate-limiting step in graft incorporation is proliferating osteoprogenitor cell recruitment

Despite obvious advantages, the use of bone allograft lags far behind autografting for the reconstruction of large skeletal defects (reviewed in [9]). Autografts contain osteoprogenitor cells, a mineralized matrix scaffold, and growth factors that collectively allow the graft to seamlessly integrate at the site of transplantation. Allografts, on the other hand, are predominantly comprised of the mineralized matrix fraction of bone that has undergone deproteinization and decellularization to ensure immune-compatibility [38]. Compared to autologous bone grafts, allografts incorporate slowly. This is not an issue of immune compatibility; rather, creeping graft incorporation is a direct result of the deproteination and decellularization steps that remove both osteoprogenitor cells and pro-osteogenic proteins.

The ingrowth of osteoprogenitor cells onto the allograft scaffold is a passive, and thus slow, process [39,40], and has been implicated as a contributing factor in the greater variability in clinical outcomes that are observed when allografts are used [41]. Since a graft must be biologically incorporated before it can be used for load-bearing purposes e.g., to support a dental implant, methods to accelerate graft incorporation have considerable clinical utility.

We gained critical insights into the problem of slow allograft incorporation: in a vertical ridge augmentation procedure (Fig. 1), we found that graft incorporation was related to the recruitment and proliferation of Wnt-responsive osteoprogenitors from the adjacent periosteum (Figs. 2,3). While bone graft particles supported the attachment of osteoprogenitor cells, they did not stimulate either their recruitment from the periosteum or enhance their proliferation (Fig. 2). Even if particles were present but the periosteum remained intact, few if any proliferating osteoprogenitor cells were detected (Supplemental Fig. 3). Clearly then, methods to increase the number and/or distribution of these proliferating progenitor cells around bone graft particles represented a rationale strategy to improve the rate of graft incorporation. Our data demonstrate that at least the initial rate of graft incorporation was accelerated in response to L-WNT3A (Fig. 4).

4.2. Bioactivating a bone graft with WNT

Wnt proteins rank amongst the most potent pro-osteogenic signals [42–44], which has directly led to the development of Wnt pathway activators for purposes of increasing bone mass [45] and accelerating bone repair [46]. For purposes of accelerating graft incorporation, however, systemic delivery of drugs such as romosozumab, an anti-Sclerostin antibody [47], is contraindicated because long-term use actually suppresses osteoprogenitor cell proliferation [48]. Therefore, we looked for methods of locally delivering WNT protein to sites requiring bone reconstruction.

Based on the size of L-WNT3A [22] and the average pore size in bovine bone graft [49], the entrapment and release of active L-WNT3A from bone graft particles (Fig. 4) probably occurred by passive diffusion. It is also likely that diffusion accounted for the transient impact that L-WNT3A had on graft incorporation and new bone formation (Fig. 4). Consequently, methods to improve L-WNT3A entrapment efficiency and to allow sustained, localized release kinetics are ongoing.

Physical encapsulation of a growth factor into a scaffold is one standard approach but this method of incorporation is inefficient and not well-suited to allogeneic bone products that do not undergo a gelation or solidification step. Another commonly used strategy is immobilization, but accumulating evidence shows that many growth factors lose their biological activity as a result [50]. When biomolecules do not adsorb to a substrate surface, then covalent immobilization of a growth factor to a material may improve release kinetics. Chemically attaching the growth factor controls an initial burst release because desorption is influenced by enzymatic or hydrolytic cleavage of the chemical bond, but such methods must also ensure that growth factor activity is not compromised (reviewed in [51]).

4.3. Vertical ridge augmentation with bone graft substitutes: room for improvement?

Within the first year following tooth extraction, up to 25 % of bone volume is lost [52]; volumetric changes continue for up to 5 years, leading to significant aesthetic and restorative challenges [53]. The characteristic thin, dense edentulous ridge seen in edentulous patients is replicated in part by the murine edentulous ridge (Fig. 1). This anatomical site in mice, however, has never supported a tooth. We compared histologic features of the human edentulous ridge with that observed in the mouse model. In both, the edentulous portion of the jawbone is considerably thinner than the tooth-bearing area (Fig. 3 and see [54]), and in both the periosteum overlying the edentulous site is osteogenic, with defects evident in the cortical bone structure (Fig. 1A,B and see [55]). In addition, both exhibit a pattern of lamellar bone with minimal marrow spaces (Fig. 1 and see [54]). Therefore, the murine edentulous ridge adequately replicates the edentulous condition in patients.

In our mouse model, the gain in vertical ridge augmentation with bone graft particles was extreme, in that the height was more than doubled (Fig. 1). In most clinical studies, an increase in human ridge height of ~19–25% (i.e. 3.85–5.14 mm) can be expected [56]. Clearly then, this rodent model represented a robust regenerative situation compared to the clinical situation. Since anatomical and histologic appearance of the human and mouse edentulous ridge appeared similar, the next most obvious difference between the two was

their age: young adult mice were employed in our study whereas most patients undergoing vertical ridge augmentation are ~50 years of age [57].

While it is formally possible that rodents are not a good model in which to evaluate methods to improve vertical ridge augmentation, the phenotype of the $Sost^{-/-}$ mutant mouse argues against this. As we showed, mice with null mutations in SOST develop significantly thicker edentulous ridges (Fig. 3); so, too, to humans carrying null mutations in SOST. Patients with van Buchem disease and sclerosteosis develop unusually thick, dense bone, which is especially pronounced in the jawbones [58,59]. Consequently, we look to better understand why in a murine model the vertical ridge augmentation was particularly successful, in hopes of improving outcomes in patients undergoing the same type of procedure.

4.4. Limitations of the study

The small size of the animal model necessitated that bone graft particles be morselized prior to their introduction into the tunnel. While some commercial vendors claim that at least some of the efficacy of their bone graft materials is related to particle size [60], we found that the morselized particles were effective at supporting osteoprogenitor cell attachment and new bone formation (Figs. 1,2). Particle size does not appear to influence the rate of new bone formation [61–63]; thus, this may not actually constitute a limitation of the current study.

5. Conclusions

Allogeneic bone grafts exploit an endogenous repair response (Fig. 2) but absent the recruitment and proliferation of osteoprogenitor cells from nearby periostea, they are ineffective (Supplemental Fig. 3). If a bioactivated allograft could trigger both the recruitment and proliferation of osteoprogenitor cells, then this would address a key deficit in allograft incorporation.

Supplementary Material

Refer to Web version on PubMed Central for supplementary material.

Acknowledgements

We thank Gunwoo Baek, Jose Vasquez and Isaiah Dawid for their help in histological analyses. This work was supported by grants from Natural Science Foundation of China (81800962), the China Scholarship Council (201806245006), Sichuan University Postdoctoral Foundation (2018SCU12015) and National Institutes of Health (R01DE02400013). All authors declare no potential conflicts of interest.

REFERENCES

[1]. Pape HC, Evans A, Kobbe P. Autologous bone graft: properties and techniques. J Orthop Trauma 2010;24 Suppl(1):S36–40. [PubMed: 20182233]

[2]. An HS, Simpson JM, Glover JM, Stephany J. Comparison between allograft plus demineralized bone matrix versus autograft in anterior cervical fusion. A prospective multicenter study. Spine (Phila Pa 1976) 1995;20(20):2211–6. [PubMed: 8545714]

[3]. Gazdag AR, Lane JM, Glaser D, Forster RA. Alternatives to autogenous bone graft: efficacy and indications. J Am Acad Orthop Surg 1995;3(1):1–8. [PubMed: 10790647]

[4]. Sakkas A, Schramm A, Winter K, Wilde F. Risk factors for post-operative complications after procedures for autologous bone augmentation from different donor sites. J Craniomaxillofac Surg 2018;46(2):312–22. [PubMed: 29233704]

[5]. Dimitriou R, Jones E, McGonagle D, Giannoudis PV. Bone regeneration: current concepts and future directions. BMC Med 2011;9:66. [PubMed: 21627784]

[6]. Chen CH, Wang L, Serdar Tulu U, Arioka M, Moghim MM, Salmon B, et al. An osteopenic/osteoporotic phenotype delays alveolar bone repair. Bone 2018;112:212–9. [PubMed: 29704698]

[7]. Kingsmill VJ, Boyde A, Jones SJ. The resorption of vital and devitalized bone in vitro: significance for bone grafts. Calcif Tissue Int 1999;64(3):252–6. [PubMed: 10024385]

[8]. Zerbo IR, de Lange GL, Joldersma M, Bronckers AL, Burger EH. Fate of monocortical bone blocks grafted in the human maxilla: a histological and histomorphometric study. Clin Oral Implants Res 2003;14(6):759–66. [PubMed: 15015953]

[9]. Sanz M, Vignoletti F. Key aspects on the use of bone substitutes for bone regeneration of edentulous ridges. Dent Mater 2015;31(6):640–7. [PubMed: 25882277]

[10]. Tuli SM, Singh AD. The osteoninductive property of decalcified bone matrix. An experimental study. J Bone Joint Surg Br 1978;60(1):116–23. [PubMed: 342532]

[11]. Shimozono Y, Hurley ET, Nguyen JT, Deyer TW, Kennedy JG. Allograft compared with autograft in osteochondral transplantation for the treatment of osteochondral lesions of the talus. J Bone Joint Surg Am 2018;100(21): 1838–44. [PubMed: 30399078]

[12]. Schmitt CM, Doering H, Schmidt T, Lutz R, Neukam FW, Schlegel KA. Histological results after maxillary sinus augmentation with Straumann(R) BoneCeramic, Bio-Oss(R), Puros(R), and autologous bone. A randomized controlled clinical trial, Clin Oral Implants Res 2013;24(5):576–85. [PubMed: 22324456]

[13]. Tilkeridis K, Touzopoulos P, Ververidis A, Christodoulou S, Kazakos K, Drosos GI. Use of demineralized bone matrix in spinal fusion. World J Orthop 2014;5(1):30–7. [PubMed: 24649412]

[14]. Chen J, Lan Y, Baek JA, Gao Y, Jiang R. Wnt/beta-catenin signaling plays an essential role in activation of odontogenic mesenchyme during early tooth development. Dev Biol (Basel) 2009;334(1):174–85.

[15]. Leucht P, Helms JA. Wnt signaling: an emerging target for bone regeneration. J Am Acad Orthop Surg 2015;23(1):67–8. [PubMed: 25538132]

[16]. Baron R, Kneissel M. WNT signaling in bone homeostasis and disease: from human mutations to treatments. Nat Med 2013;19(2):179–92. [PubMed: 23389618]

[17]. Gaur T, Lengner CJ, Hovhannisyan H, Bhat RA, Bodine PV, Komm BS, et al. Canonical WNT signaling promotes osteogenesis by directly stimulating Runx2 gene expression. J Biol Chem 2005;280(39):33132–40. [PubMed: 16043491]

[18]. Chen Q, Cao HZ, Zheng PS. LGR5 promotes the proliferation and tumor formation of cervical cancer cells through the Wnt/beta-catenin signaling pathway. Oncotarget 2014;5(19):9092–105. [PubMed: 25193857]

[19]. Song L, Liu M, Ono N, Bringhurst FR, Kronenberg HM, Guo J. Loss of wnt/beta-catenin signaling causes cell fate shift of preosteoblasts from osteoblasts to adipocytes. J Bone Miner Res 2012;27(11):2344–58. [PubMed: 22729939]

[20]. Regard JB, Zhong Z, Williams BO, Yang Y. Wnt signaling in bone development and disease: making stronger bone with Wnts. Cold Spring Harb Perspect Biol 2012; 4(12).

[21]. Weivoda MM, Youssef SJ, Oursler MJ. Sclerostin expression and functions beyond the osteocyte. Bone 2017;96:45–50. [PubMed: 27888056]

[22]. Dhamdhere GR, Fang MY, Jiang J, Lee K, Cheng D, Olveda RC, et al. Drugging a stem cell compartment using Wnt3a protein as a therapeutic. PLoS One 2014;9(1):e83650. [PubMed: 24400074]

[23]. Zhao L, Rooker SM, Morrell N, Leucht P, Simanovskii D, Helms JA. Controlling the in vivo activity of Wnt liposomes. Methods Enzymol 2009;465:331–47. [PubMed: 19913175]

[24]. Morrell NT, Leucht P, Zhao L, Kim JB, ten Berge D, Ponnusamy K, et al. Liposomal packaging generates Wnt protein with in vivo biological activity. PLoS One 2008;3(8):e2930. [PubMed: 18698373]

[25]. Takada R, Satomi Y, Kurata T, Ueno N, Norioka S, Kondoh H, et al. Monounsaturated fatty acid modification of Wnt protein: its role in Wnt secretion. Dev Cell 2006;11(6):791–801. [PubMed: 17141155]

[26]. Plonka AB, Urban IA, Wang HL. Decision tree for vertical ridge augmentation. Int J Periodontics Restorative Dent 2018;38(2):269–75. [PubMed: 29447321]

[27]. Yuan X, Pei X, Zhao Y, Tulu US, Liu B, Helms JA. A wnt-responsive PDL population effectuates extraction socket healing. J Dent Res 2018:22034518755719.

[28]. Tu X, Delgado-Calle J, Condon KW, Maycas M, Zhang H, Carlesso N, et al. Osteocytes mediate the anabolic actions of canonical Wnt/beta-catenin signaling in bone. Proc Natl Acad Sci U S A 2015;112(5):E478–86. [PubMed: 25605937]

[29]. Filali M, Cheng N, Abbott D, Leontiev V, Engelhardt JF. Wnt-3A/beta-catenin signaling induces transcription from the LEF-1 promoter. J Biol Chem 2002;277(36):33398–410. [PubMed: 12052822]

[30]. Cadigan KM. TCFs and Wnt/beta-catenin signaling: more than one way to throw the switch. Curr Top Dev Biol 2012;98:1–34. [PubMed: 22305157]

[31]. Smale ST. Luciferase assay. Cold Spring Harb Protoc 2010;5(2010), pdb prot5421.

[32]. Bouxsein ML, Boyd SK, Christiansen BA, Guldberg RE, Jepsen KJ, Muller R. Guidelines for assessment of bone microstructure in rodents using micro-computed tomography. J Bone Miner Res 2010;25(7):1468–86. [PubMed: 20533309]

[33]. Yuan X, Pei X, Zhao Y, Li Z, Chen CH, Tulu US, et al. Biomechanics of immediate postextraction implant osseointegration. J Dent Res 2018;97(9):987–94. [PubMed: 29608868]

[34]. Wang YL, Hong A, Yen TH, Hong HH. Isolation of mesenchymal stem cells from human alveolar periosteum and effects of vitamin d on osteogenic activity of periosteum-derived cells. J Vis Exp 2018;(135).

[35]. Debnath S, Yallowitz AR, McCormick J, Lalani S, Zhang T, Xu R, et al. Discovery of a periosteal stem cell mediating intramembranous bone formation. Nature 2018;562(7725):133–9. [PubMed: 30250253]

[36]. Hassler N, Roschger A, Gamsjaeger S, Kramer I, Lueger S, van Lierop A, et al. Sclerostin deficiency is linked to altered bone composition. J Bone Miner Res 2014;29(10):2144–51. [PubMed: 24753092]

[37]. Wu Y, Yuan X, Perez KC, Hyman S, Wang L, Pellegrini G, et al. Aberrantly elevated Wnt signaling is responsible for cementum overgrowth and dental ankylosis. Bone 2019;122:176–83. [PubMed: 30408613]

[38]. Stopa Z, Siewert-Gutowska M, Abed K, Szubinska-Lelonkiewicz D, Kaminski A, Fiedor P. Evaluation of the safety and clinical efficacy of allogeneic bone grafts in the reconstruction of the Maxilla and mandible. Transplant Proc 2018;50(7):2199–201. [PubMed: 30177136]

[39]. Burchardt H The biology of bone graft repair. Clin Orthop Relat Res 1983;(174):28–42.

[40]. Roberts TT, Rosenbaum AJ. Bone grafts, bone substitutes and orthobiologics: the bridge between basic science and clinical advancements in fracture healing. Organogenesis 2012;8(4):114–24. [PubMed: 23247591]

[41]. Frohlich M, Grayson WL, Wan LQ, Marolt D, Drobnic M, Vunjak-Novakovic G. Tissue engineered bone grafts: biological requirements, tissue culture and clinical relevance. Curr Stem Cell Res Ther 2008;3(4):254–64. [PubMed: 19075755]

[42]. Liu Y, Li Z, Arioka M, Wang L, Bao C, Helms JA. WNT3A accelerates delayed alveolar bone repair in ovariectomized mice. Osteoporos Int 2019;30(9):1873–85. [PubMed: 31338519]

[43]. Chen T, Li J, Cordova LA, Liu B, Mouraret S, Sun Q, et al. A WNT protein therapeutic improves the bone-forming capacity of autografts from aged animals. Sci Rep 2018;8(1):119. [PubMed: 29311710]

[44]. Salmon B, Liu B, Shen E, Chen T, Li J, Gillette M, et al. WNT-activated bone grafts repair osteonecrotic lesions in aged animals. Sci Rep 2017;7(1):14254. [PubMed: 29079746]

[45]. Genant HK, Engelke K, Bolognese MA, Mautalen C, Brown JP, Recknor C, et al. Effects of romosozumab compared with teriparatide on bone density and mass at the spine and hip in postmenopausal women with low bone mass. J Bone Miner Res 2017;32(1):181–7. [PubMed: 27487526]

[46]. Minear S, Leucht P, Jiang J, Liu B, Zeng A, Fuerer C, et al. Wnt proteins promote bone regeneration. Sci Transl Med 2010;2(29), 29ra30.

[47]. Saag KG, Petersen J, Brandi ML, Karaplis AC, Lorentzon M, Thomas T, et al. Romosozumab or alendronate for fracture prevention in women with osteoporosis. N Engl J Med 2017;377(15):1417–27. [PubMed: 28892457]

[48]. Boyce RW, Brown D, Felx M, Mellal N, Locher K, Pyrah I, et al. Decreased osteoprogenitor proliferation precedes attenuation of cancellous bone formation in ovariectomized rats treated with sclerostin antibody. Bone Rep 2018;8: 90–4. [PubMed: 29955626]

[49]. Figueiredo M, Henriques J, Martins G, Guerra F, Judas F, Figueiredo H. Physicochemical characterization of biomaterials commonly used in dentistry as bone substitutes–comparison with human bone. J Biomed Mater Res B Appl Biomater 2010;92(2):409–19. [PubMed: 19904820]

[50]. Ziegler J, Anger D, Krummenauer F, Breitig D, Fickert S, Guenther KP. Biological activity of recombinant human growth factors released from biocompatible bone implants. J Biomed Mater Res A 2008;86(1):89–97. [PubMed: 17941024]

[51]. Li J, Mooney DJ. Designing hydrogels for controlled drug delivery. Nat Rev Mater 2016;1(12).

[52]. Schropp L, Wenzel A, Kostopoulos L, Karring T. Bone healing and soft tissue contour changes following single-tooth extraction: a clinical and radiographic 12-month prospective study. Int J Periodontics Restorative Dent 2003;23(4):313–23. [PubMed: 12956475]

[53]. Pietrokovski J, Starinsky R, Arensburg B, Kaffe I. Morphologic characteristics of bony edentulous jaws. J Prosthodont 2007;16(2), 141–147. [PubMed: 17362425]

[54]. Kingsmill VJ. Post-extraction remodeling of the adult mandible. Crit Rev Oral Biol Med 1999;10(3):384–404. [PubMed: 10759415]

[55]. Krajicek DD, Dooner J, Porter K. Observations on the histologic features of the human edentulous ridge. Part III: Bone, J Prosthet Dent 1984;52(6):836–43. [PubMed: 6595394]

[56]. Elnayef B, Monje A, Gargallo-Albiol J, Galindo-Moreno P, Wang HL, Hernandez-Alfaro F. Vertical ridge augmentation in the atrophic mandible: a systematic review and meta-analysis. Int J Oral Maxillofac Implants 2017;32(2):291–312. [PubMed: 28291849]

[57]. Chavda S, Levin L. Human studies of vertical and horizontal alveolar ridge augmentation comparing different types of bone graft materials: a systematic review. J Oral Implantol 2018;44(1):74–84. [PubMed: 29135351]

[58]. Stephen LX, Hamersma H, Gardner J, Beighton P. Dental and oral manifestations of sclerosteosis. Int Dent J 2001;51(4):287–90. [PubMed: 11570544]

[59]. Schendel SA. Van Buchem disease: surgical treatment of the mandible. Ann Plast Surg 1988;20(5):462–7. [PubMed: 3377422]

[60]. Arbez B, Kun-Darbois JD, Convert T, Guillaume B, Mercier P, Hubert L, et al. Biomaterial granules used for filling bone defects constitute 3D scaffolds: porosity, microarchitecture and molecular composition analyzed by microCT and Raman microspectroscopy. J Biomed Mater Res B Appl Biomater 2019;107(2):415–23. [PubMed: 29675998]

[61]. Miron RJ, Hedbom E, Saulacic N, Zhang Y, Sculean A, Bosshardt DD, et al. Osteogenic potential of autogenous bone grafts harvested with four different surgical techniques. J Dent Res 2011;90(12):1428–33. [PubMed: 21940523]

[62]. Pallesen L, Schou S, Aaboe M, Hjorting-Hansen E, Nattestad A, Melsen F. Influence of particle size of autogenous bone grafts on the early stages of bone regeneration: a histologic and stereologic study in rabbit calvarium. Int J Oral Maxillofac Implants 2002;17(4):498–506. [PubMed: 12182292]

[63]. Zaner DJ, Yukna RA. Particle size of periodontal bone grafting materials. J Periodontol 1984;55(7):406–9. [PubMed: 6086869]

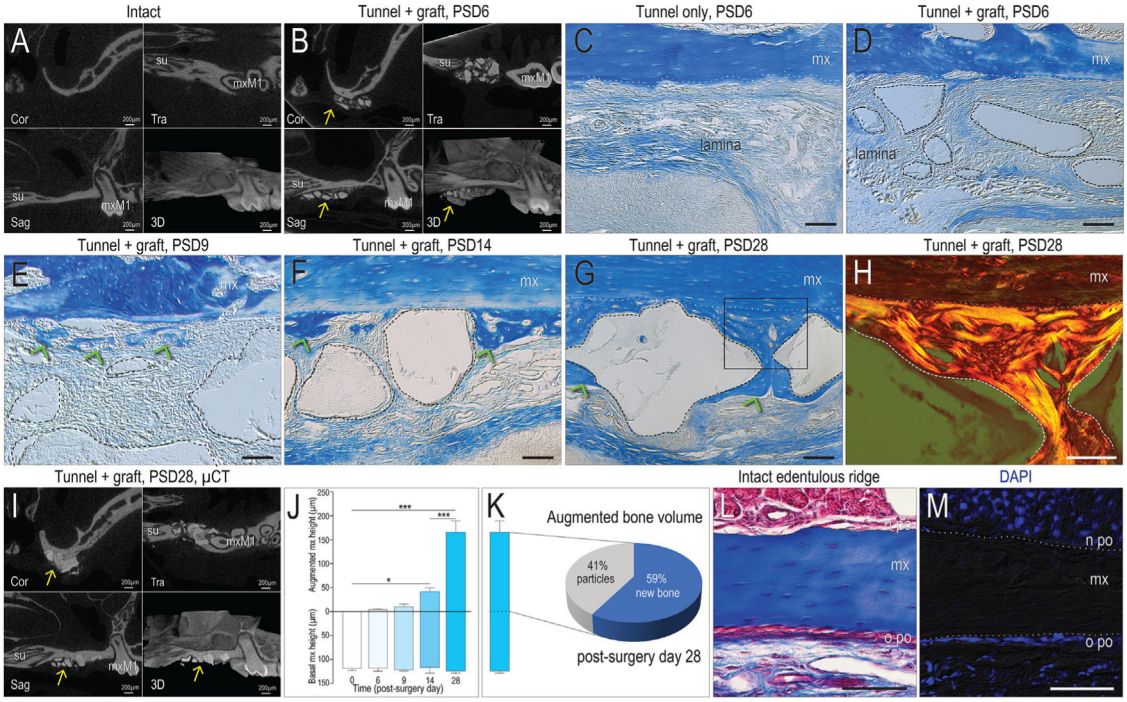

Fig. 1 –.

A rodent model of vertical ridge augmentation with bone graft. µCT scanning and 3D reconstruction of the maxillary edentulous ridge in the (A) intact state and (B) 6 days following placement of a bone graft between the maxillary bone and the periosteum. Aniline blue staining of representative tissue sections through the maxillary edentulous ridge on PSD6 following (C) a tunneling procedure; and (D) a tunneling procedure plus bone grafting; dotted white line indicates the border of the maxillary bone; dashed black lines indicate borders of the graft particles. A tunneling procedure plus bone grafting, on (E) PSD9, (F) PSD14, and (G) PSD28; green arrow heads indicate the newly formed bone. (H) Picrosirius red staining of the near-adjacent tissue section of G; dashed white lines indicate borders of the bone graft particles. (I) µCT scanning and 3D reconstruction of the maxillary edentulous ridge 28 days following the grafting. (J) Histomorphometric quantification of the maxillary edentulous ridge basal bone height and augmented bone height. (K) Pie chart showing the fraction of bone graft in total augmented area in grafted mice 28 days following the grafting. (L) Masson's trichrome staining of a representative tissue section through the intact maxillary edentulous ridge illustrating the maxillary periostea. (M) DAPI staining to detect cell nuclei. The dotted white lines demarcate the edges of the maxillary bone. Abbreviations: mxM1, maxillary first molar; Cor, coronal plane; Tra, transaxial plane; Sag, sagittal plane; su, suture; mx, maxilla; o po, oral periosteum; n po, nasal periosteum. Scale bars: 50 µm if not indicated.

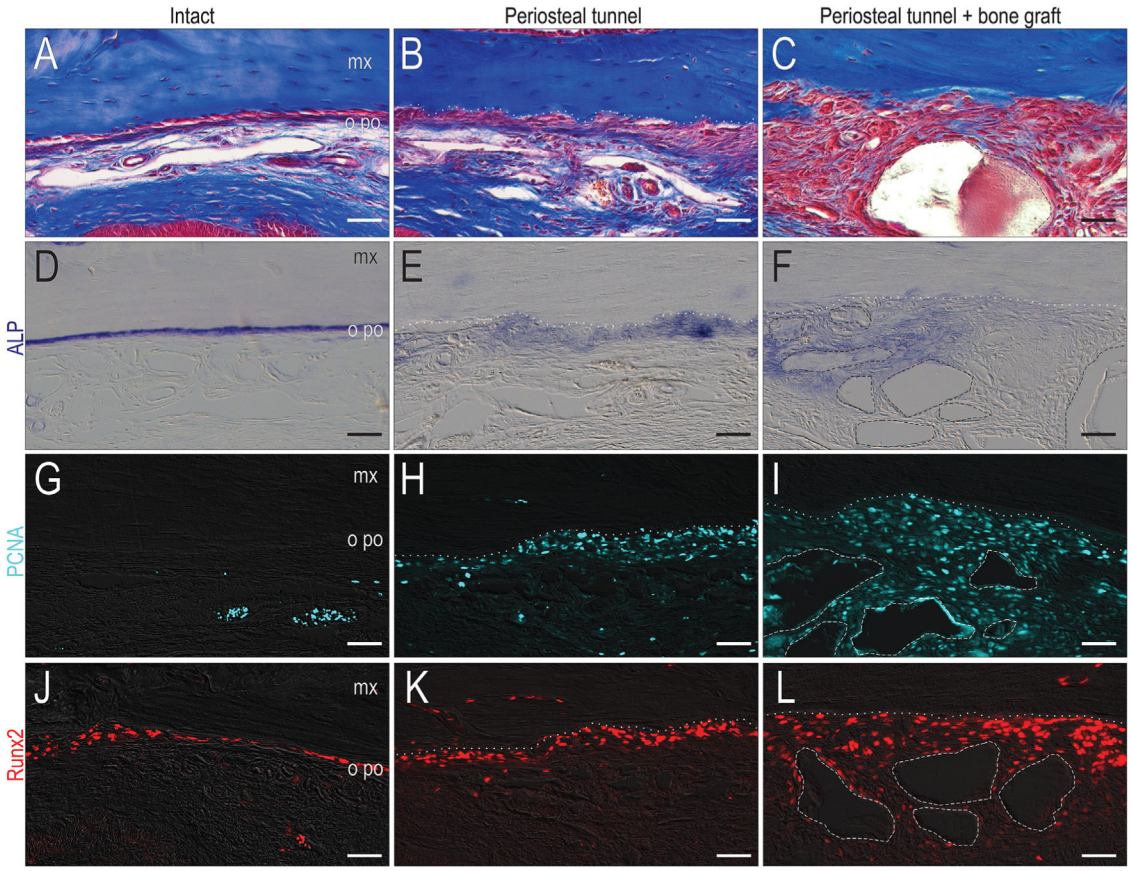

Fig. 2 –.

A tunneling procedure activates osteoprogenitor cell proliferation. Masson trichrome staining of representative tissue sections through the maxillary edentulous ridge (A) in the intact state and on PSD6 following (B) a tunneling procedure and (C) a tunneling procedure plus bone grafting. ALP activity in the (D) intact periosteum, versus ALP activity 6 days following (E) a minimally invasive tunnel procedure and (F) a tunneling and bone grafting. In a near-adjacent tissue section, PCNA immunostaining in the (G) intact periosteum, versus on PSD6 following (H) a tunneling procedure and (I) a tunneling procedure plus bone grafting. Runx2 immunostaining in the (J) intact periosteum, versus on PSD6 following (K) a tunneling procedure and (L) a tunneling procedure plus bone grafting. Abbreviations and dotted and dashed lines: as in Fig. 1. Scale bars: 50 μm.

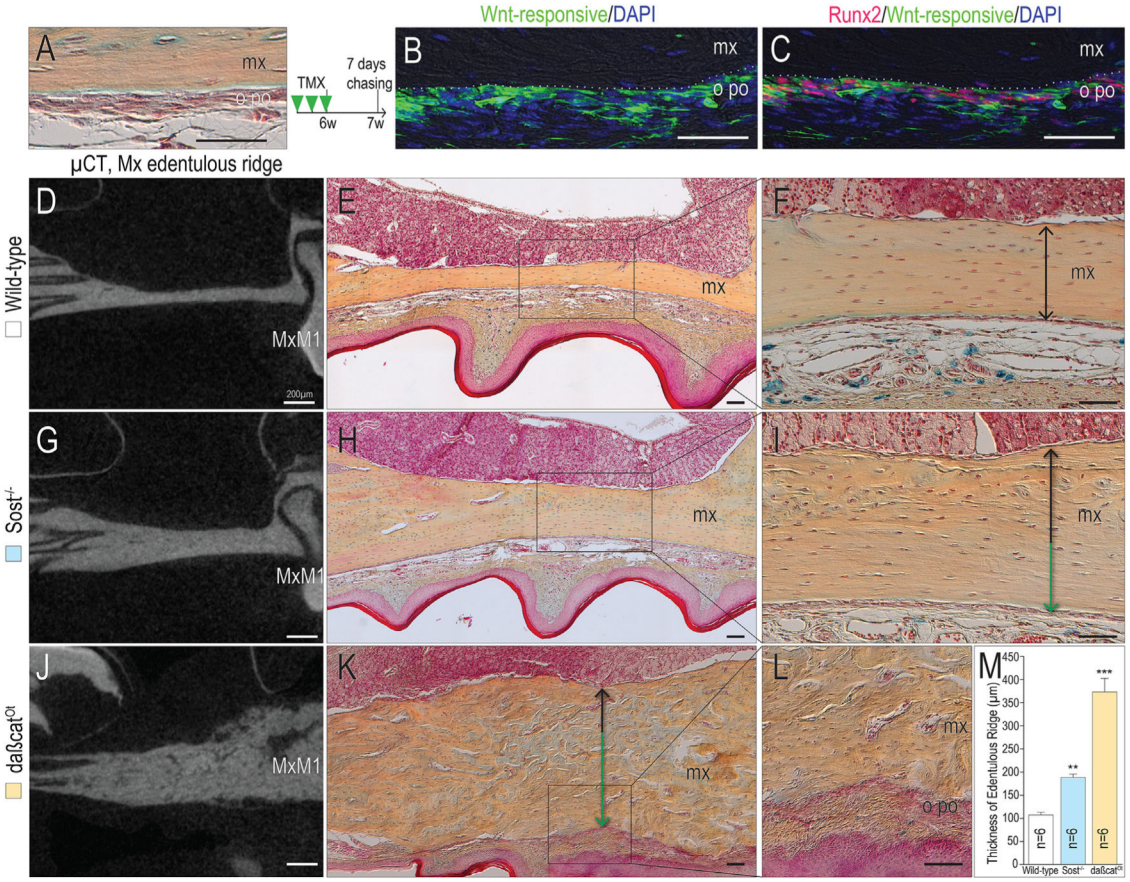

Fig. 3 –.

Upregulated Wnt signaling resulted in high bone mass. (A) Pentachrome staining illustrating the intact maxillary periosteum of oral surface. (B) GFP immunostaining of the near-adjacent tissue section of A indicating the distribution of Wnt-responsive cells. (C) Merged GFP and Runx2 co-staining of B. (D) Representative sagittal section of μCT scanning of the maxillary edentulous ridge and (E, F) pentachrome staining of a representative tissue section through the same site in wild-type control mice. Representative (G) μCT section and (H, I) pentachrome staining of a tissue section in Sost$^{-/-}$ mice. Representative (J) μCT section and (K, L) pentachrome staining of a tissue section in daßcat^{Ot} mice. (M) Quantification of the maxillary edentulous ridge basal bone height. (O) ALP activity and (P) Runx2 immunostaining of the near-adjacent tissue section of L; (Q) ALP activity and (R) Runx2 immunostaining of the near-adjacent tissue section of M. Black double-headed arrows indicate the maxillary edentulous ridge basal bone height of wild-type mice, while green arrows indicate the increased height. Abbreviations, dotted lines: as in Fig. 1. Scale bars: 50 μm if not indicated.

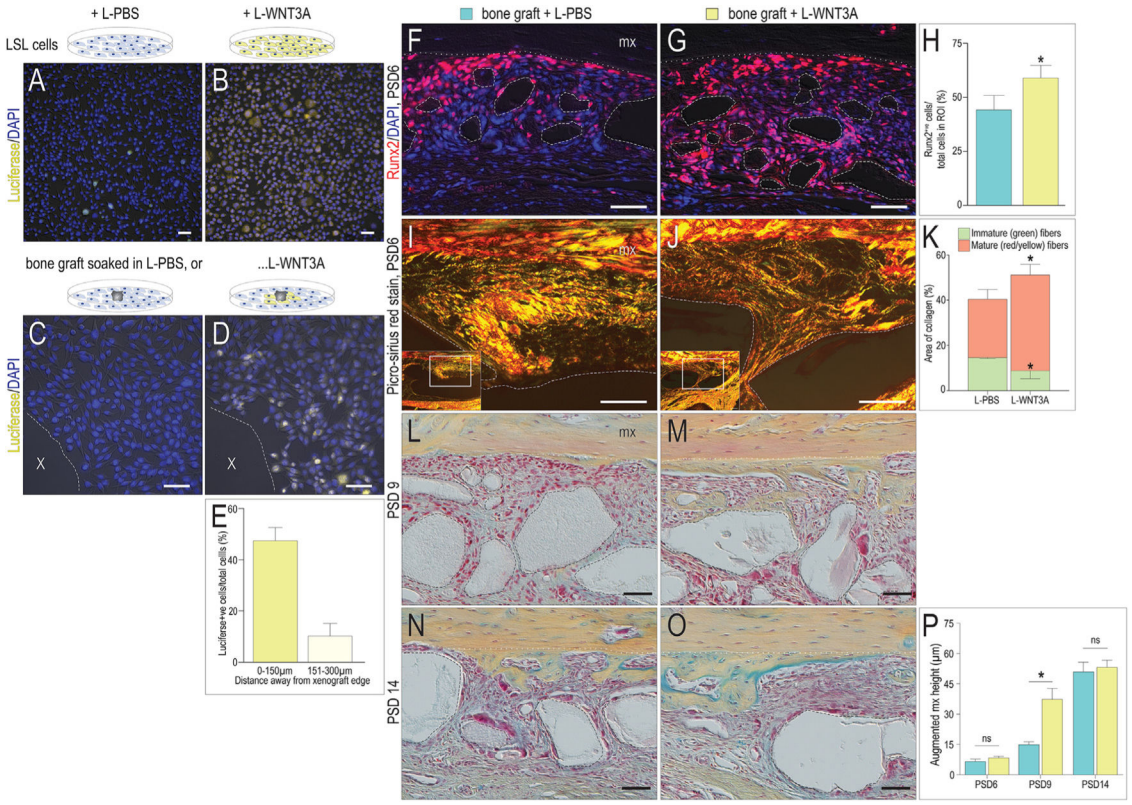

Fig. 4 –.

WNT3A accelerates the onset of new bone formation. LSL cells, identified by DAPI staining, were interrogated using IHC for luciferase expression following treatment with (A) L-PBS or (B) L-WNT3A. LSL cells were treated with bone graft particles soaked in (C) L-PBS or (D) L-WNT3A. (E) Quantification of Wnt activity in response to L-WNT3A delivered via bone graft particles. IHC localization of Runx2 (red signal) and DAPI (blue signal) on representative tissue sections through the maxillary edentulous ridge on PSD6 following a transplantation of graft in combination with a (F) L-PBS or (G) L-WNT3A. (H) Quantification of the percentage of $Runx2^{+ve}$ cells/total cells in a ROI, centered on the graft particles. Picrosirius red staining showing collagen fiber organization around graft particles treated with (I) L-PBS or (J) L-WNT3A. (K) Quantification of green pixels (corresponding to immature collagen fibers) and red/yellow pixels (corresponding to mature fibers) in the total area around the graft particles (see Methods). Pentachrome staining showing the maxillary edentulous ridge on PSD9 following (L) L-PBS- or (M) L-WNT3A-combined grafting. Pentachrome staining showing the maxillary edentulous ridge on PSD14 following (N) L-PBS- or (O) L-WNT3A-combined grafting. (P) Histomorphometric quantification of the augmented bone height in L-PBS and L-WNT3A groups. Abbreviations, dotted lines and dashed lines: as in Fig. 1. Scale bars: 50 μm.